OUTCOMES OF PLANET-SCALE COLLISIONS. R. M. Canup[1] and E. Asphaug[2], [1]Southwest Research Institute; 1050 Walnut Street, Suite 426; Boulder, CO 80302; robin@boulder.swri.edu; [2]Earth Sciences Department, University of California; Santa Cruz, CA 95064; asphaug@es.ucsc.edu.

Introduction: Collisions between planet-sized bodies, *i.e.* those larger than a few thousand kilometers, are believed to dominate the final stages of terrestrial accretion (*e.g.,* [1]). One such impact is believed responsible for the origin of the Moon [2], [3]. Current parameterizations for the outcomes of planet-scale impacts are limited, and rely either on extrapolations from laboratory or numerical experiments involving smaller objects (*e.g.,* [4]-[6]), or on results of simulations of lunar-forming impacts [7]. Here we have utilized a smoothed-particle hydrodynamics (SPH) method to conduct an initial set of simulations of collisions between planet-sized bodies. The dependencies of the mass and angular momentum contained in orbiting debris on the colliding mass and collision angular momentum are considered.

Method: The SPH simulation utilized here is a variant of a code by Benz (*e.g.* [8]) which employs a tree code for gravitational interactions, a variable smoothing length, and artificial viscosity for shocks. Internal strength of the objects is ignored, a valid assumption for the size-range of interest here [4]. The energy budget is determined by shock heating, ($P\,dV$) work, and the equation of state (in this case, the Tillotson EOS is used as in [4]); radiative transfer is not included.

For laboratory-scale scenarios, SPH has been gauged against known impact results with exceptional fidelity [9]. However, there are regimes for which SPH is not well suited, and its application could yield potentially unphysical results. Caution is thus required in choosing astrophysical problems and interpreting the validity of results. A good example is the accretion of a moon from a torus of ejected melt and vapor, in which a hypervelocity impact takes place at enormous impact energy, followed by cooling and coagulation of the ejected material placed into orbit. While the production of bound debris may be a result robustly obtained via SPH given an appropriate equation of state (see below), the long-term evolution of that bound debris requires the integration of additional physics (*e.g.*, radiative transfer in a melt/vapor torus, viscous dissipation and angular momentum transport in a disk) which is currently not adequately addressed by the SPH code utilized here.

Initial Conditions: Here we consider collisions between objects with a two-component core-mantle structure. We create our initial protoplanets by first simulating the head-on collision of an iron impactor into a basalt target, with an impact velocity equal to the mutual escape velocity of the two objects, with $v_{esc}^2 = 2G(M_1 + M_2)/(R_1 + R_2)$ and $v_\infty = 0$. The mass of iron is set at 30% of the total colliding mass. While the colliding iron and rock objects are not initially in compressional equilibrium, the end result is a self-differentiated and collisionally heated basalt/iron protoplanet composed of approximately N =10,000 particles in equilibrium. The protoplanets created in this manner are used as the targets and impactors in our simulations, so that each run involves a total of about N =20,000 particles (*e.g.,* Fig. 1).

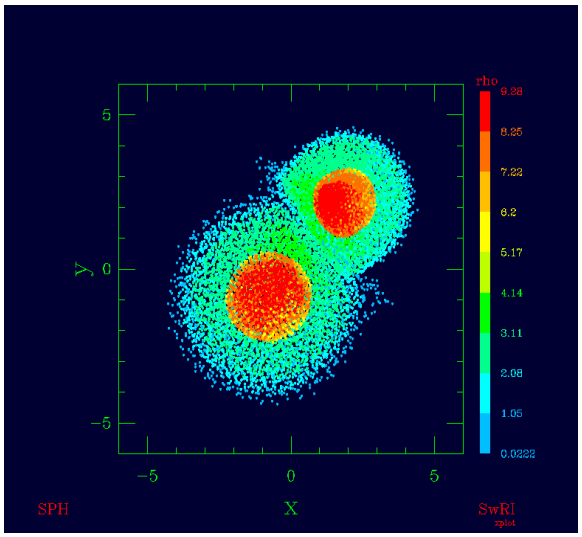

Fig. 1: An early time step from an oblique impact between two differentiated basalt-iron bodies whose relative velocity is in the x-direction. Color scales with density.

The impact simulations performed here involve varying impact velocities (v_{imp}/v_{esc} = 1, 1.2, 1.5 and 2.0), total colliding masses (M_T = 0.1 and $0.9M_\oplus$), and impact parameters ($b/(R_1 + R_2) = 0 \rightarrow 0.8$). All used an impactor to total mass ratio of $\gamma = 0.3$ (the same as in [10]); each impact was followed for about 1 day of simulated time, or ~ 10^2 gravitational time scales, where $\tau_{grav} \sim (R_1 + R_2)/v_{esc}$. This is also a similar time period to that tracked in [10], and by visual inspection is sufficient in these cases to allow for the target to assume a regular, oblate spheroidal shape. It should be noted that the issues of interest here (*e.g.* the mass of bound debris) are dynamic quantities, and their values continue to evolve somewhat over time for longer runs (*e.g.,* [10], his Fig. 6).

Production of bound debris: The first group of 8 simulations whose results we report here involved oblique impacts and (v_{imp}/v_{esc}) = 1 and 1.2; these are the types of impacts which have previously been shown to leave material in bound orbits (*e.g.,* [11]). At the end of a simulation, we classify all particles as 1) escaping, 2) orbiting, or 3) contained within the protoplanet. Escaping particles are those with positive total energies (kinetic + potential). We classify a particle as being in bound orbit if its total energy is negative, and its angular momentum exceeds that of a circular

Keplerian orbit at the surface of the protoplanet. In some instances, particularly those producing substantial vapor, the surface of the protoplanet after the collision is not clearly defined. We therefore use an analytic method to solve for the mass and radius of the resulting protoplanet in an attempt to maintain as consistent of a comparison as possible across different simulations. First, an initial estimate of the fraction of mass contained in the protoplanet is used to calculate the amount of escaping and bound debris; conservation of mass then yields an updated value for the planet's mass. The planet's radius is then defined by assuming a terrestrial average density. This procedure is repeated iteratively until convergence is achieved; a similar approach was used to generate the results in [7].

Recent lunar-forming impact simulations (*e.g.,* [10], [11]) have utilized the equation of state known as ANEOS, and consider dunite-iron impactors and targets. In [7], results of these simulations were examined, and it was found that the fraction of the total mass (M_T) placed into bound orbits, (M_D/M_T), and the fraction of angular momentum contained in this material, (L_D/L_*), is a function of the impact angular momentum, L, scaled by a quantity L_*, as shown in Fig. 2. Here L_* is the critical angular momentum for rotational stability for an object with mass M_T, with $(L/L_*) \equiv \sqrt{2} f(\alpha) \sin\xi / K$, where K is the gyration constant (0.335 for the Earth), ξ is the angle of the impact trajectory to the local surface normal, and $f(\alpha) = \gamma(1-\gamma)\sqrt{\gamma^{1/3} + (1-\gamma)^{1/3}}$ where $\gamma = M_{imp}/M_T$. Fig. 2 also shows results from 8 of our new runs (open circles & squares). Despite the use of a different equation of state and a different material (dunite vs. basalt), the results obtained here are broadly similar to those of Cameron. In particular, the observed variation of the amount of angular momentum contained in bound debris as a function of (L/L_*) shown in (b) is quite consistent in both sets.

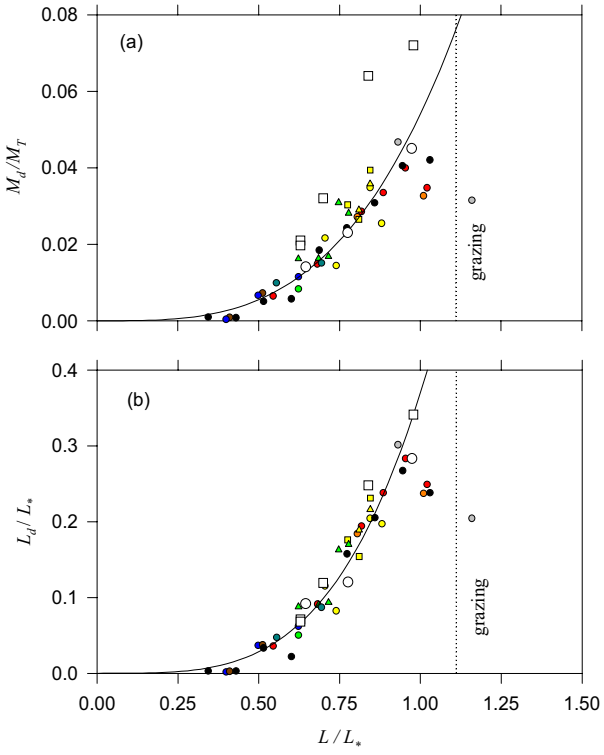

Fig. 2: Results from simulations performed here (open circles & squares) vs. those from [10] (color symbols). (a) Orbiting mass/Total mass vs. impact angular momentum, L, scaled by L_*. (b) Angular momentum of orbiting material scaled by L_* vs. (L/L_*). The solid curves are fits to Cameron's data from [7]; the vertical line corresponds to the grazing limit for γ = 0.3.

A notable feature of our results to date is a proportionally greater amount of orbiting mass produced in simulations involving $M_T = 0.9M_\oplus$ (open squares in Fig. 2) vs. that obtained in simulations involving $M_T = 0.1M_\oplus$ (open circles), as well as that found by [10]. For the $0.9M_\oplus$ mass collisions, we observe a greater degree of vaporization than is found in Cameron's simulations that involve a similar mass. Since the codes are similar, the difference is most likely due to differences inherent to the EOS and/or initial conditions. The current version of ANEOS utilized in [10] requires material to attain the enthalpy of dissociation into a monatomic species [12]-[13], leading to a significant underestimation of vaporization. Conversely, the Tillotson EOS used here does not handle a two-phase melt/vapor well, and does not account for the latent heat of melting. In addition, the impactors and targets we used were collisionally generated, so that more massive targets/projectiles had initially higher energies than their smaller counterparts; in contrast, Cameron initialized his objects to 2000K, irrespective of total mass or depth. Further work beyond the few preliminary simulations shown here will be necessary to account for these differences and to assess the expected physical state of the orbiting material.

References: [1] Agnor, C.B., Canup, R.M. & H.F. Levison (1999) *Icarus* 142, 219-237. [2] Hartmann, W.K. & Davis, D.R. (1975) *Icarus* 24, 504-515. [3] Cameron, A.G.W. & Ward, W.R. (1976) *LPSC VII,* 120-122. [4] Benz, W. & Asphaug, E. (1999) *Icarus* 142, 5-20. [5] Melosh, H.J. & Ryan, E. (1997) *Icarus* 129, 562-564. [6] Housen, K.R. & Holsapple, K.A. (1990) *Icarus* 84, 226-253. [7] Canup, R.M., Ward, W.R. & Cameron, A.G.W. (2001), *Icarus*, in press. [8] Benz, W., Slattery, W. L. & Cameron, A.G.W. (1986) *Icarus* 66, 515-535. [9] Benz, W. & Asphaug, E. (1994) *Icarus* 107, 98. [10] Cameron, A.G.W. (2000) In *Origin of the Earth and Moon*, Eds. R.M. Canup & K. Righter, 133-144. [11] Cameron, A.G.W. & Benz, W. (1991) *Icarus* 92, 165-168. [12] Pierazzo, E. & Melosh, H.J. (1997) *LPSC XXIX,* 935. [13] Melosh, H.J. (1999) *fall AGU meeting.*